Available online at www.sciencedirect.com
SCIENCE DIRECT®
PHYSICS LETTERS A
ELSEVIER
Physics Letters A 308 (2003) 381–390
www.elsevier.com/locate/pla

Stability analysis for the synchronization of semiconductor lasers with ultra-high frequency current modulation

Y. Chembo Kouomou [a,b], P. Woafo [a,*]

[a] *Laboratoire de Mécanique, Faculté des Sciences, Université de Yaoundé I, B.P. 812 Yaoundé, Cameroon*
[b] *Division of Technical Telecommunication Studies, Minpostel, Yaoundé, Cameroon*

Received 22 April 2002; received in revised form 20 November 2002; accepted 8 January 2003

Communicated by A.P. Fordy

Abstract

We study the nonlinear dynamics of ultra-high frequency current-modulated semiconductor lasers. A retroactive coupling scheme is applied to achieve their synchronization both in the regular and chaotic regimes. The stability analysis is performed to determine the suitable coupling parameters leading to high-quality synchronization. The consequences of parameter mismatch are also highlighted. Numerical simulations confirm the analytic approach.

1. Introduction

The synchronization of chaotic oscillators has gathered an increasing interest during this last decade [1–3]. Applications in the fields of biology, physics and engineering rapidly appeared to be wide. As far as communication engineering is concerned, chaotic synchronization is expected to ensure a high-level privacy for telecommunications and data transfer [4–6]. Consequently, intense research activities are actually conducted for the synchronization of semiconductor lasers (laser diodes) which are currently the standard optoelectronic emitter–receiver systems in fiber-optics networks (see Ref. [7] and references therein).

The rate equations describing semiconductor lasers usually possess only two degrees of freedom, namely, the photon and carrier densities. Hence, additional degrees of freedom should artificially be introduced for chaos to appear. For that purpose, a first method uses an external reflector to feed back into the active layer of the laser diode a fraction of its delayed electromagnetic output. Thereby, the infinite dimensionality created by the feedback delay induces an hyperchaotic dynamics which is sometimes referred to as coherence collapse [8]. In this Letter, we will rather consider a second alternative which generates chaos through the amplitude modulation of the injection current. The chaotic behavior of these high-frequency Current-Modulated Semiconductor Lasers (CMSLs) has yet been studied both theoretically and experimentally [9–12].

In view of practical applications, several key issues still require deeper investigations. Amongst them,

* Corresponding author.
E-mail address: pwoafo@uycdc.uninet.cm (P. Woafo).

0375-9601/03/$ – see front matter
doi:10.1016/S0375-9601(03)00070-7

the stability analysis of the synchronization process particularly gathers a lot of attention [13–17]. Even though few techniques have recently been developed and can serve as interesting guidelines, the determination of the suitable coupling parameters (i.e., those which induce a robust and quasi-perfect synchronization) is a difficult problem which commonly resists to analytic approaches. On the other hand, the unavoidable parameter mismatches can constitute a serious threat for the accuracy of synchronization, as it may subject the figurative phase point to intermittent burst-like repulsions from the synchronization manifold [18–21]. The aim of this Letter is therefore to explain how the variation of the various parameters does influence the stability of the master–slave CMSLs system for a particular type of unidirectional coupling. We will also examine the impact of parameter mismatch on the quality of synchronization.

The Letter is organized as follows. In Section 2, we first focus on the chaotic dynamics and bifurcation behavior of uncoupled CMSLs. We also present the unidirectional coupling which will ensure the synchronization both in the regular and chaotic regimes. The stability analysis is performed in Section 3. Floquet theory will enable us to give a qualitative interpretation of the various stability and instability intervals that can be observed as the coupling parameter is increased. Section 4 will deal with the effects of parameter mismatch upon the maximum synchronization error, which is the most constraining indicator of the synchronization quality. At last, we conclude in Section 5.

The numerical simulation of all ordinary differential equations is performed with the fourth-order Runge–Kutta algorithm, and the nonlinear algebraic equations are solved with the Newton–Raphson algorithm.

2. Dynamics and synchronization of current-modulated semiconductor lasers

As we have earlier noticed, the relevant variables for semiconductor lasers are the photon density P and the carrier density N. Considering the amplitude modulation of the injection current, the rate equations read

$$\frac{\mathrm{d}P}{\mathrm{d}t} = \left[g(N-N_0)(1-sP) - \frac{1}{\tau_p}\right]P + \frac{\beta N}{\tau_s},$$
$$\frac{\mathrm{d}N}{\mathrm{d}t} = I(t) - \frac{N}{\tau_s} - g(N-N_0)(1-sP)P. \tag{1}$$

The meaning and numerical values of the various parameters are resumed in Table 1. We have assumed that

$$I(t) = I_b + I_m \sin(2\pi f_m t), \tag{2}$$

where I_b and I_m are, respectively, the bias and modulation currents, while f_m is the modulation frequency. A suitable normalization of Eqs. (1) leads to the following dimensionless form

$$\dot{p} = \big[(1+2n)(1-\sigma p) - 1\big]p + \beta(n+\Phi),$$
$$\dot{n} = \varepsilon\big[i_0\big(1+m\sin(\omega t)\big) - n - (1+2n)(1-\sigma p)p\big], \tag{3}$$

with the following rescalings

$$\varepsilon = \frac{\tau_p}{\tau_s}, \quad \sigma = \frac{s}{g\tau_s/2}, \quad \Phi = \frac{1}{2}gN_{\mathrm{th}}\tau_p,$$

Table 1
Parameter values used for the numerical simulations

Symbol	Parameter	Value
g	Gain coefficient	$8.4\times10^{-13}\ \mathrm{m^3\,s^{-1}}$
s	Nonlinear gain suppression factor	$0.5\times10^{-26}\ \mathrm{m^3}$
β	Spontaneous emission coefficient	10^{-5}
N_{th}	Carrier density at threshold	$2.018\times10^{24}\ \mathrm{m^{-3}}$
N_0	Carrier density at transparency	$1.435\times10^{24}\ \mathrm{m^{-3}}$
τ_s	Carrier lifetime	1.025 ns
τ_p	Photon lifetime	2.041 ps
I_{th}	Threshold injection current density	$1.969\times10^{33}\ \mathrm{m^{-3}\,s^{-1}}$
f_m	Frequency of the modulation current	2 GHz

$$i_0 = \Phi\frac{I_b - I_{\text{th}}}{I_{\text{th}}}, \quad m = \frac{I_m}{I_b - I_{\text{th}}}, \quad \omega = 2\pi f_m \tau_p,$$
$$p = \left(\frac{1}{2} g \tau_s\right) P, \quad n = \frac{1}{2} g N_{\text{th}} \tau_p \left(\frac{N}{N_{\text{th}}} - 1\right). \tag{4}$$

The dots over p and n in Eqs. (3) denote the derivative relatively to the reduced time (in units of τ_p). One should note that the dimensionless injection current $i(t)$ is now characterized by its time average amplitude i_0 and its modulation index m.

For certain parameter values, the CMSL exhibits a chaotic behavior. Fig. 1(a) displays the chaotic oscillations of the photon density p as a function of time. They are constituted of spikes with randomly distributed amplitudes, alternatively followed by irregular bursts of quite smaller amplitudes. This two-frequency structure is also foreshadowed in the phase plane of Fig. 1(b), where one can notice that the chaotic attractor intrinsically possesses the characteristic notch of double-periodic oscillations. It also appears on the bifurcation diagrams of Figs. 2(a) and (b) that chaos occurs when the CMSL is strongly excited, i.e., for high i_0 or m. More precisely, chaos seems to be possible only when the modulation index approximately exceeds 0.95. In both cases, the route to chaos is the period-doubling cascade of pitchfork bifurcations.

The synchronization of CMSLs can be carried out through different methods. For example, a bidirectional coupling has recently been used to synchronize such lasers [22]. In that case, the synchronized CMSLs were going from chaotic to periodic behavior through

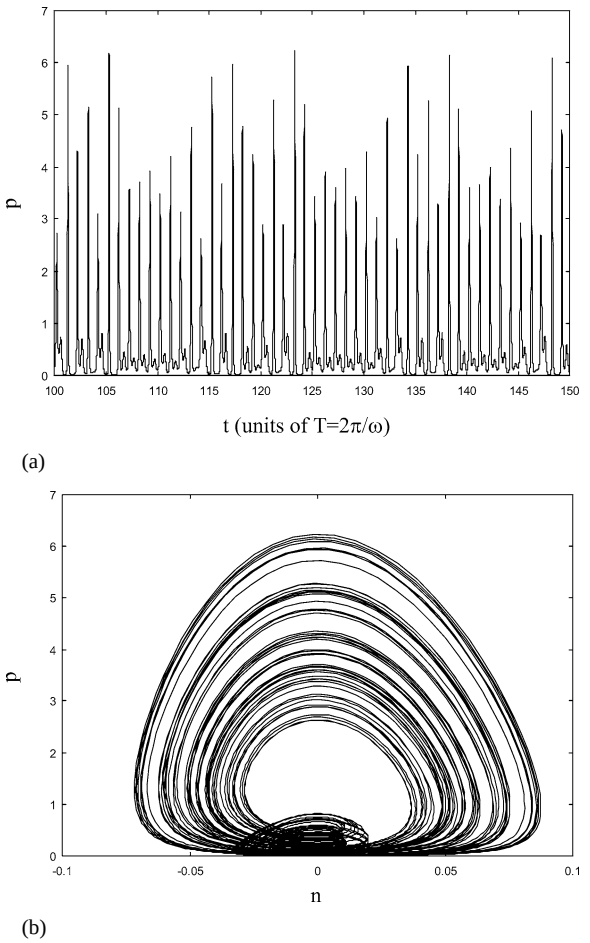

Fig. 1. (a) Chaotic behavior of the CMSL for $i_0 = 0.6$ and $m = 1.0$; (b) Corresponding phase plane.

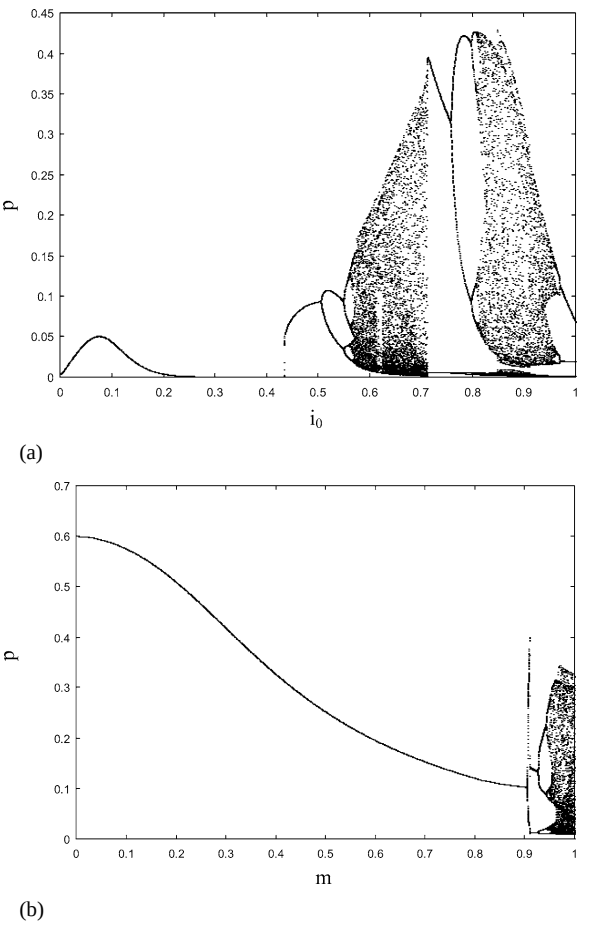

Fig. 2. Bifurcation diagrams: (a) For i_0 with $m = 1.0$; (b) For m with $i_0 = 0.6$.

a reverse period-doubling sequence as the coupling parameter was increased. In this Letter, we will rather use a retroactive coupling scheme [23,24], which can be explicitly written in vectorial notation as

$$\begin{aligned}\dot{\mathbf{x}} &= \mathbf{F}(\mathbf{x}, t),\\ \dot{\tilde{\mathbf{x}}} &= \mathbf{F}(\tilde{\mathbf{x}}, t) - \mathbf{C}(\tilde{\mathbf{x}} - \mathbf{x}),\end{aligned} \tag{5}$$

where the tilde ($\sim$) indicates the slave variables, while the vector-flows **F** and **C**, respectively, describe the uncoupled CMSL and the unidirectional coupling. The state vector is obviously $\mathbf{x} \equiv (p, n)$ in our case. Here, we aim to use a feedback coupling which physically corresponds to a situation where a current proportional to the difference of the slave and master output powers is electronically fed to the slave CMSL, so that the slave rate equations may be expressed according to

$$\begin{aligned}\dot{\tilde{p}} &= \big[(1+2\tilde{n})(1-\sigma\tilde{p}) - 1\big]\tilde{p} + \beta(\tilde{n} + \Phi),\\ \dot{\tilde{n}} &= \varepsilon\big[i_0\big(1 + m\sin(\omega t)\big) - K(\tilde{p} - p) - \tilde{n}\\ &\qquad - (1+2\tilde{n})(1-\sigma\tilde{p})\tilde{p}\big],\end{aligned} \tag{6}$$

where K is a scalar parameter. When convergence requirements are met, this coupling forces the slave system to duplicate the dynamics of the master. This is clearly demonstrated by the diagonal synchronization manifold on Fig. 3. The following section will therefore focus on the conditions under which the coupling efficiently completes a robust and high-quality synchronization.

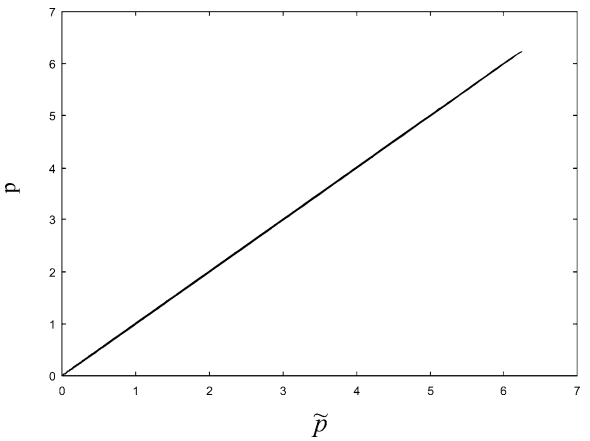

Fig. 3. Synchronization manifold of the master–slave system for $i_0 = 0.6$ and $m = 1.0$. The coupling strength has been fixed to $K = 5.0$.

3. Stability of the synchronization manifold

The stability analysis of synchronized nonlinear oscillators is commonly carried out through the study of the asymptotic behavior of the deviation vector (whose Euclidian norm is the synchronization error)

$$\mathbf{w}(t) = \tilde{\mathbf{x}}(t) - \mathbf{x}(t), \tag{7}$$

which estimates the instantaneous mutual proximity between the master and slave sub-systems in the phase plane. In general, depending on the coupling parameter(s), three distinct situations can arise from the stability study according to the value of $\mathbf{w}(t)$ as $t \to +\infty$. The first of them occurs when $\|\mathbf{w}(+\infty)\| = 0$. In that case, the slave trajectory progressively degenerates to the master one, and consequently stable synchronization is achieved. The second situation arises when $0 < \|\mathbf{w}(+\infty)\| < +\infty$, i.e., when the synchronization error does not converge to zero and does not diverge to infinity either. Here, the synchronization is said to have failed, since the **x** and $\tilde{\mathbf{x}}$ oscillations remain uncorrelated despite the coupling. The third and last situation corresponds to $\|\mathbf{w}(+\infty)\| = +\infty$, i.e., the coupling induces a sustained growth to infinity for the slave system variables. This situation is obviously worst than the second, as it can lead to catastrophic consequences. We aim in this section to determine under which conditions each of these three configurations is observed in our system. There is no need to stress anymore the extreme importance of such a study in view of practical applications.

At a linear approximation, the deviation vector obeys to

$$\dot{\mathbf{w}} = \left[\left(\frac{\partial \mathbf{F}}{\partial \tilde{\mathbf{x}}}\right)_{\mathbf{w}=0} - \left(\frac{\partial \mathbf{C}}{\partial \tilde{\mathbf{x}}}\right)_{\mathbf{w}=0}\right] \cdot \mathbf{w} = \mathbf{J}(\mathbf{x}, t) \cdot \mathbf{w}. \tag{8}$$

As we have earlier noticed, synchronization is achieved when the Jacobian matrix $\mathbf{J}(\mathbf{x}, t)$ drives **w** to **0** at long term. For this situation to occur, it is known that the so-called sub-Lyapunov exponents should necessarily be negative [1]. Unfortunately, these exponents can only be derived numerically, and thus do not give any analytic insight into the stability analysis problem. Therefore, several propositions have been made to surmount that deficiency. The most straightforward is to suppose that stability can be ensured if the Jacobian matrix $\mathbf{J}(\mathbf{x}, t)$ has uniformly negative eigenvalues throughout the whole chaotic

attractor, but this assumption has recently been proved to be invalid [15]. Other stability constraints have later been proposed, either based on Lyapunov functions [18] or on the decomposition of $\mathbf{J}(\mathbf{x},t)$ into its time average and time varying components [19]. Even though the consequent stability constraints have the merit to be analytic and mathematically rigorous, they are unfortunately overly strong for certain dynamical systems, and they commonly fail to reproduce the complex stability patterns which are obtained through experiments and numerical simulations.

In this Letter, we generalize an approach which has successfully been applied to the particular case of single-well Duffing oscillators [16]. In fact, Eq. (8) resists to exact analytic treatments because the Jacobian is a function of the vector $\mathbf{x}$, which is a chaotic variable. To circumvent this problem, we will replace this chaotic variable $\mathbf{x}$ by $\mathbf{x}^0$, which is here assumed to be the most probable Unstable Periodic Orbit (UPO) intrinsically embedded within the chaotic attractor, and which like $\mathbf{x}$ also obeys to

$$\dot{\mathbf{x}}^0 = \mathbf{F}(\mathbf{x}^0, t). \tag{9}$$

Since $\mathbf{x}^0$ is a priori multiperiodic, it can be expanded in Fourier series as

$$\mathbf{x}^0(t) = \sum_{k=0}^{+\infty} \big[\mathbf{A}_k \cos(k\omega t) + \mathbf{B}_k \sin(k\omega t)\big]. \tag{10}$$

The parametric modulation frequency ω has logically been considered as the base of our multiperiodic expansion. Therefore, the Fourier components $\mathbf{A}_k$ and $\mathbf{B}_k$ can be recovered through the Ritz variational criterion according to

$$\int_0^{2\pi/\omega} \big[\dot{\mathbf{x}}^0 - \mathbf{F}(\mathbf{x}^0, t)\big] e^{jk\omega t}\, dt = 0, \quad k = 0, 1, 2, \ldots, \tag{11}$$

j being the unit complex number. Finally, the stability analysis is resumed to the following Floquet problem

$$\dot{\mathbf{w}} = \mathbf{J}(\mathbf{x}^0, t) \cdot \mathbf{w}. \tag{12}$$

The difference between Eqs. (12) and (8) is that the stability of the synchronization manifold is now investigated through the Floquet exponents rather than the conventional sub-Lyapunov exponents.

The master and slave CMSLs are described by two sets of two first-order Ordinary Differential Equations (ODEs) each. For mathematical commodity, we will transform them into a single set of two second-order ODEs. Therefore, if we discard σ and β because of their very small order of magnitude ($\sim 10^{-5}$), the rate equations can now be expressed as

$$\begin{aligned}
&\ddot{p} + \varepsilon(1+2p)\dot{p} - 2\varepsilon p\big[i_0(1+m\sin\omega t) - p\big] \\
&\quad - \dot{p}^2/p = 0, \\
&\ddot{\tilde{p}} + \varepsilon(1+2\tilde{p})\dot{\tilde{p}} \\
&\quad - 2\varepsilon\tilde{p}\big[i_0(1+m\sin\omega t) - K(\tilde{p}-p) - \tilde{p}\big] \\
&\quad - \dot{\tilde{p}}^2/\tilde{p} = 0.
\end{aligned} \tag{13}$$

The synchronization error will consequently be defined as the following scalar variable

$$u = \tilde{p} - p, \tag{14}$$

which obeys at a linear approximation to

$$\begin{aligned}
&\ddot{u} + \left[\varepsilon(1+2p) - \frac{2\dot{p}}{p}\right]\dot{u} \\
&\quad + \left[2\varepsilon\big(\dot{p} + (K+2)p - i_0(1+m\sin\omega t)\big) + \frac{\dot{p}^2}{p^2}\right]u = 0.
\end{aligned} \tag{15}$$

Note that this latter equation corresponds to Eq. (8). The chaotic variable may now be replaced by its corresponding UPO p^0. Therefore, if we straightforwardly consider the multiperiodicity of p^0, the stability analysis will require the resolution of a differential equation with a multifrequency parametric excitation. Even though the related study would logically yield the most satisfying results, it should be noticed that unfortunately, the consequent analytical stability boundaries can hardly be derived in that case, even within the frame of perturbation theory.

In fact, previous studies have demonstrated that such a complexity can be avoided when the chaotic attractor is almost simply folded, i.e., looks like a simple closed loop in the phase space. It has been shown in [15] for Rössler oscillators and in [16] for single-well Duffing oscillators that for such chaotic attractors, a single period-one UPO is sufficient to describe accurately the stability pattern of the master–slave coupled system. Since the chaotic attractor of the CMSL is an almost simply folded band in the phase plane (p,n), we aim to derive the stability

pattern of the coupled system with a unique single-frequency truncated UPO, that is, we approximate the multiperiodic orbit p^0 with only its constant and fundamental spectral components as follows

$$p^0(t) = A_0 + A_1 \cos\omega t + B_1 \sin\omega t. \tag{16}$$

In Eq. (15), $\dot{p}$ and $\dot{p}^2$ can be neglected in the parametric excitation terms, since they are, respectively, proportional to ω (of order ε) and ω^2 (of order ε^2). Moreover, the parametric damping is of order ε, while the stiffness term is proportional to $\sqrt{\varepsilon}$. Hence, the parametric damping can be replaced by its time average value

$$\lambda = \big\langle \varepsilon(1+2p) \big\rangle = \varepsilon(1+2A_0). \tag{17}$$

According to the Ritz variational criterion, A_0, A_1 and B_1 obey to the following set of nonlinear algebraic equations:

$$\begin{aligned}
&-\omega^2 A_1 + \lambda B_1 \omega + 4\varepsilon A_0 A_1 - 2\varepsilon i_0 A_1 = 0,\\
&-\omega^2 B_1 - \lambda A_1 \omega + 4\varepsilon A_0 B_1 - 2\varepsilon i_0 B_1 - 2\varepsilon m i_0 A_0 = 0,\\
&2A_0^2 + A_1^2 + B_1^2 - 2i_0 A_0 - m i_0 B_1 = 0,
\end{aligned} \tag{18}$$

and Eq. (15) may now be rewritten as

$$\ddot{u} + \lambda \dot{u} + \big\lfloor \Omega_0^2 + \mu \cos(\omega t - 2\varphi) \big\rfloor u = 0 \tag{19}$$

with

$$\begin{aligned}
&\Omega_0^2 = 2\varepsilon\big[(K+2)A_0 - i_0\big],\\
&\mu = 2\varepsilon\Big[\big((K+2)A_1\big)^2 + \big((K+2)B_1 - m i_0\big)^2\Big]^{1/2}.
\end{aligned} \tag{20}$$

This latter equation can be transformed into the canonical Mathieu equation

$$\frac{\mathrm{d}^2\eta}{\mathrm{d}\tau^2} + \big[\delta + 2\alpha\cos(2\tau - 2\varphi)\big]\eta = 0 \tag{21}$$

with the following rescalings

$$\begin{aligned}
&\tau = \frac{\omega \mathrm{t}}{2}; \quad \eta = u \exp\left(\frac{\lambda\tau}{\omega}\right),\\
&\delta = \frac{4}{\omega^2}\left[\Omega_0^2 - \frac{\lambda^2}{4}\right], \quad \alpha = \frac{2\mu}{\omega^2}.
\end{aligned} \tag{22}$$

The solution of the Mathieu equation has the form [25]

$$\eta(\tau) = \mathrm{e}^{\theta\tau}\phi(\tau) \tag{23}$$

where θ is a complex number, and ϕ a π-periodic function. According to Eqs. (22), the synchronization is stable when $\Re[\theta] < \lambda/\omega$, and unstable otherwise. Therefore, the stability domain is analytically delimited as [16]

$$-\sinh^2\left(\frac{\lambda\pi}{2\omega}\right) < \Gamma(\delta,\alpha) < +\cosh^2\left(\frac{\lambda\pi}{2\omega}\right), \tag{24}$$

where Γ is the real function defined as

$$\Gamma(\delta,\alpha) = \begin{cases} \Delta(0)\sin^2\big(\frac{1}{2}\pi\sqrt{\delta}\big) & \text{if } \delta \geqslant 0,\\ -\Delta(0)\sinh^2\big(\frac{1}{2}\pi\sqrt{-\delta}\big) & \text{if } \delta < 0, \end{cases} \tag{25}$$

and $\Delta(0)$ is the infinite Hill determinant at $\theta = 0$. With the $\delta_{k,l}$ Kronecker coefficients, this determinant can be expressed under the following symbolic form [16]

$$\Delta(0) = \left\| \delta_{k,l} - \frac{\alpha}{\delta - (2k)^2}\big(\mathrm{e}^{2\mathrm{j}\varphi}\delta_{k,l-1} + \mathrm{e}^{-2\mathrm{j}\varphi}\delta_{k,l+1}\big) \right\| \tag{26}$$

with k and l varying from $-\infty$ to $+\infty$. On the (δ,α) parametric plane, which is sometimes referred to as the Strutt diagram, the curves of equation $\Gamma(\delta,\alpha) = -\sinh^2(\lambda\pi/2\omega)$ represent the π-periodic transitions from stability to instability (and vice-versa), while the curves $\Gamma(\delta,\alpha) = +\cosh^2(\lambda\pi/2\omega)$ represent the 2π-periodic boundaries. Hence, these two types of boundaries delimit the zone of linear stability (where $u(+\infty) = 0$, i.e., where high-quality synchronization occurs). This zone is approximately represented by the shaded area in Fig. 4 [25,26]. The second zone that can be noticed on the Strutt diagram is the area of instability where any perturbation diverges to infinity ($|u(+\infty)| = +\infty$), and this area is in blank on the stability map. At last, there is a buffer zone of nonlinear stability between the linearly stable and unstable areas where $0 < |u(+\infty)| < +\infty$ (desynchronization). This latter zone (which is, however, linearly unstable) has been lightly shaded and cannot be predicted from the conventional Floquet analysis, since it is originated from the nonlinear variational terms we have discarded in Eqs. (15) (see also Ref. [25]).

From Eqs. (20) and (22), it clearly appears that when K is increased, the parameters δ and α are simultaneously varied. More specifically, the figurative

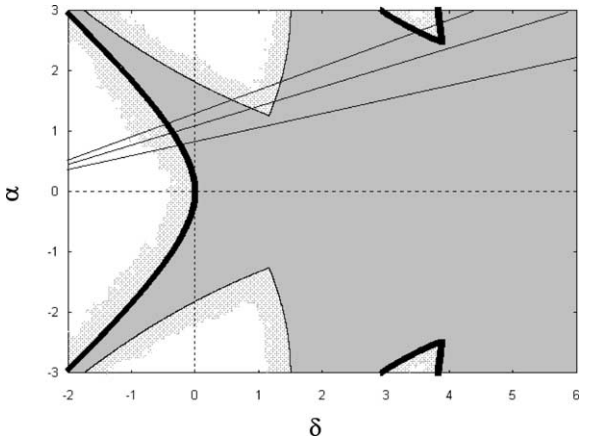

Fig. 4. Stability map in the (δ, α) parametric plane (or Strutt diagram), showing the π-periodic boundaries (thick lines) and the 2π-periodic boundaries (thin lines). Three straight lines of different slopes have been sketched, and they represent the linear approximations of the curve of Eq. (27) for increasing values of the modulation index m.

point in the (δ, α) plane sketches a curve of equation

$$\alpha = \left(\frac{1}{2}\delta + \frac{4\varepsilon i_0}{\omega^2}\right)\sqrt{\frac{A_1^2 + B_1^2}{A_0^2}} \times \left[1 + \frac{m^2 i_0^2 - \frac{2mi_0 B_1}{8\varepsilon A_0}(\omega^2\delta + 8\varepsilon i_0)}{\frac{A_1^2+B_1^2}{64\varepsilon^2 A_0^2}(\omega^2\delta + 8\varepsilon i_0)^2}\right]^{1/2}, \quad (27)$$

In first approximation, this curve can be assimilated to a straight line of slope

$$a = \frac{1}{2}\sqrt{\frac{A_1^2 + B_1^2}{A_0^2}}. \quad (28)$$

This slope is proportional to the ratio between the amplitude of the varying component of $p^0(t)$ and the amplitude of its constant component. Therefore, a is an increasing function of the modulation index m, since a stronger parametric excitation of the CMSL leads to higher A_1 and B_1 values. As K is increased, the figurative point in the Strutt diagram moves from left to right on the curve of Eq. (27), and therefore alternatively passes through linearly unstable and linearly stable areas. Consequently, the synchronization intervals for K can be represented under the form $]K_{b1}, K_{b2}[$, $]K_{b3}, K_{b4}[, \ldots,]K_{bn}, +\infty[$, where the K_{bk} are the boundary values. It appears from Fig. 4 that when m is small, the slope of the curve (27) is weak, and then the synchronization pattern is made of a single interval $]K_{b1}, +\infty[$. But as m is increased, this curve intersects the zones of linear instability because of its greater slope, so that the former single stability interval splits into an increasing number of different synchronization sub-intervals. In Fig. 4, we have graphically represented three straight lines with distinct slopes, corresponding to different values of m. From the smallest to the highest slope, these lines, respectively, lead to one, two and three synchronization intervals for K. Note that as we have earlier noticed, high values of m precisely correspond to the synchronization of CMSLs in their chaotic regime, so that complex stability patterns may be expected in that case.

It results from the above reasoning that the period-one UPO approximation predicts the progressive occurrence of compact desynchronization intervals as the modulation index m is increased. Moreover, it synthetically provides the related geometrical explanation through the Strutt diagram interpretation. Therefore, one can expect that these compact intervals of non-synchronized behavior should emerge and widen on the K-axis as m is continuously increased.

The numerical simulations completely confirm our analytic stability analysis. In Fig. 5, we have represented the maximal synchronization error as a function of the coupling strength, for increasing values of the modulation index. The maximal synchronization error we have tolerated for high-quality synchronization is 10^{-5}. Therefore, synchronization intervals are indicated on Fig. 5 by horizontal segments of equation $\log_{10}(\|\mathbf{w}\|_{\max}) = -5$. In Fig. 5(a), for example, m is quite small ($m = 0.1$), so that we have a single synchronization interval $]-1.00, +\infty[$. For $K < -1.00$, the slave variables indefinitely grow to infinity, while for $K > -1.00$, quasi-perfect synchronization is achieved. $K = -1.00$ is a boundary value for which a high (but not infinite) synchronization error is noticed. In Fig. 5(b), m has been increased ($m = 0.4$), as well as the slope of the figurative curve on the Strutt diagram. This curve now intersects a nonlinear stability area, thereby splitting the former semi-infinite interval of linear stability into two, which are $]-1.00, -0.73[$ and $]-0.67, +\infty[$. Nevertheless, the inner nonlinear stability interval obviously represents a loss of synchronization, and not a growth to infinity. When m is further increased ($m = 0.6$), the first stability interval splits into two in its turn in

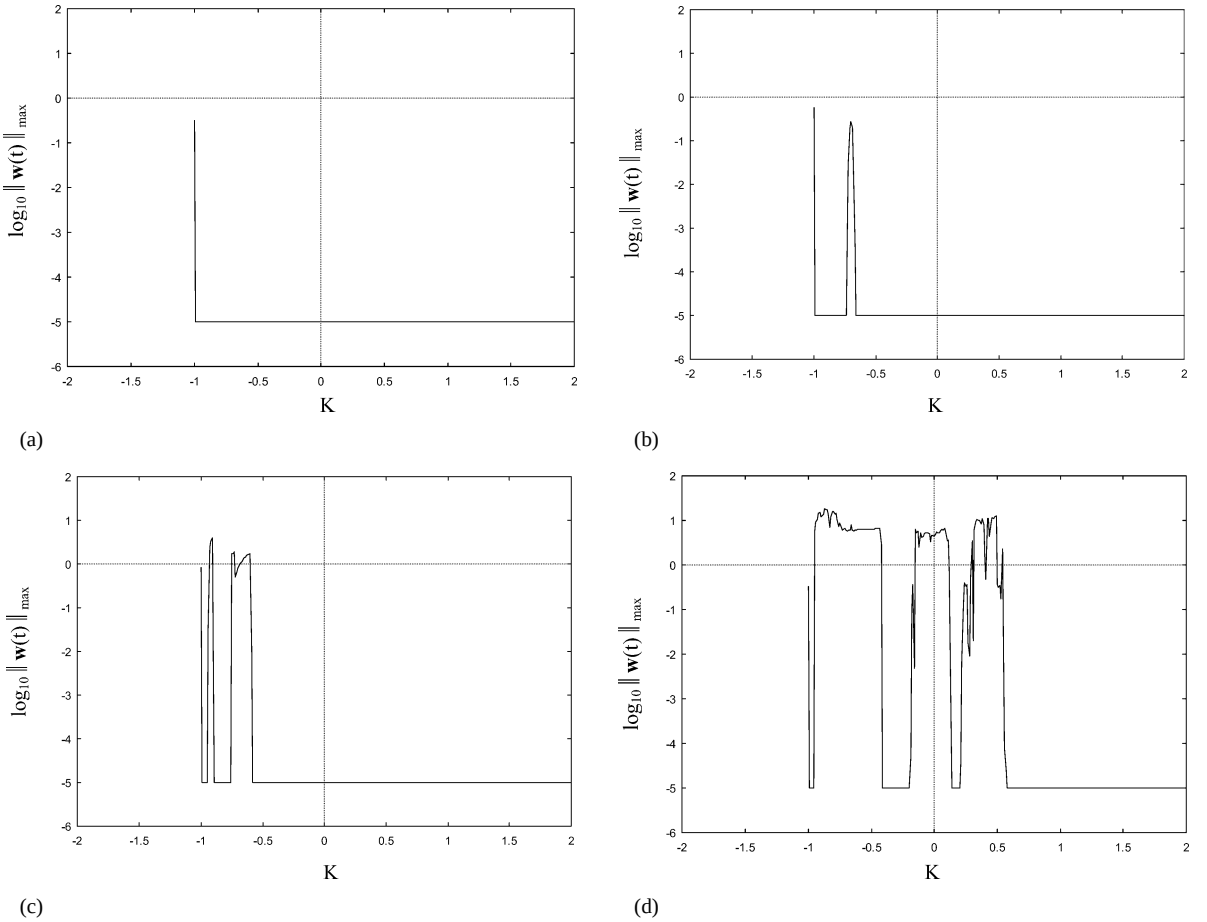

Fig. 5. Synchronization error as a function of the coupling strength K, when i_0 is fixed to 0.6. (a) $m = 0.1$; (b) $m = 0.4$; (c) $m = 0.6$; (d) $m = 1.0$. Note the progressive occurrence and widening of compact desynchronization intervals as m is increased.

Fig. 5(c), so that the stability pattern for K is now $]-1.00, -0.95[$, $]-0.90, -0.75[$ and $]-0.59, +\infty[$. According to the bifurcation diagram of Fig. 2(b), these three m values correspond to periodic oscillations. Hence, the synchronization which occurs here (even for $K = 0$) is due to phase-locking. We increase again m to 1.0 in Fig. 5(d) so that we are now synchronizing the CMSLs in their chaotic regime. The stability pattern is now made of four sub-sets which are $]-1.00, -0.95[$, $]-0.42, -0.19[$, $]0.13, 0.21[$ and $]0.57, +\infty[$. It should be noticed that the desynchronization intervals are larger in the chaotic state than in the periodic regime, and that obviously no synchronization occurs when $K = 0$. Moreover, synchronization is always ensured for the K values which are slightly above the π-periodic threshold value $K = -1.00$. This can easily be explained by the stability diagram of Fig. 4, and also from Eqs. (13), since $K = -1.00$ is the critical value that induces the inversion of the retroactive coupling term. The mechanism characterized by the progressive occurrence of desynchronization intervals through the splitting into two of a synchronization interval has invariably been observed for various sets of CMSL parameters during numerical simulations. Anyway, it has been noticed that the first instability interval $]-\infty, K_{b1}[$ always leads to a sustained growth to infinity for the slave variables, and should therefore be absolutely avoided. On the other hand, the inner instability intervals do not induce such a catastrophic behavior, but just fail to achieve stable

and robust synchronization. This can be explained by the fact that these intervals are only weakly unstable, so that the nonlinear terms of the rate equations succeed to confine the figurative phase point within the chaotic attractor when it is repelled from the linearly unstable synchronization manifold.

4. Synchronization of mismatched current-modulated semiconductor lasers

Even though parameter mismatch is unavoidable in practice, its undesirable consequences can be limited when certain optimization requirements are met [21]. If we consider the various CMSLs parameters ζ_i and their corresponding parameter mismatches $\delta\zeta_i$, the deviation vector obeys at a linear approximation to the following integral equation

$$\mathbf{w}(t) = \boldsymbol{\Theta}(t)\boldsymbol{\Theta}^{-1}(t_0)\cdot\mathbf{w}(t_0) + \int_{t_0}^{t}\left[\boldsymbol{\Theta}(t)\boldsymbol{\Theta}^{-1}(\tau) \times\left(\sum_i \frac{\partial\mathbf{F}(\mathbf{x},t,\zeta)}{\partial\zeta_i}\delta\zeta_i\right)(\tau)\right]\mathrm{d}\tau, \quad (29)$$

where $\boldsymbol{\Theta}$ is the principal matrix function, that is the solution of

$$\dot{\boldsymbol{\Theta}} = \mathbf{J}(\mathbf{x},t)\cdot\boldsymbol{\Theta}. \quad (30)$$

The first term of Eq. (29) decays to $\mathbf{0}$ as $t\to+\infty$ within the stability area. The second term does never vanish and hence corresponds to the synchronization error due to the parameter mismatch. If λ_{av} is the average largest sub-Lyapunov exponent (obviously negative), it can be demonstrated from Eq. (29) that for initially stable synchronization, $\|\mathbf{w}(t)\|_{\max}$ increases with the mismatches $|\delta\zeta_i|$, but is inversely proportional to $|\lambda_{\mathrm{av}}|$, i.e., the synchronization error is minimized when $(-\lambda_{\mathrm{av}})$ is the largest possible [21]. On Fig. 6, we have plotted the synchronization error as a function of the coupling strength K for different percentages of parameter mismatch in the chaotic regime. It is seen that in stable intervals, $\|\mathbf{w}(t)\|_{\max}$ effectively increases with the parameter mismatch. We also remark that the first stability interval (just at the right of the boundary value $K=-1.0$) is the least stable, since in that area, synchronization is lost for a parameter mismatch of only 1%. Anyway, above 1%, severe degradation of synchronization has been noticed. We are therefore led to the conclusion that the synchronization of chaotic CMSLs is very sensitive to parameter mismatch, because for other dynamical systems, a tolerance at up to 50% is sometimes witnessed. It is also very important to stress that no detuning has been applied between the modulation frequencies of the master and slave CMSLs. In fact, numerical simulations have indicated that even a detuning of 10^{-5}% destroys the synchronized state. Therefore, a quasi-perfect stabilization of these ultra-high frequencies will be necessary for practical applications.

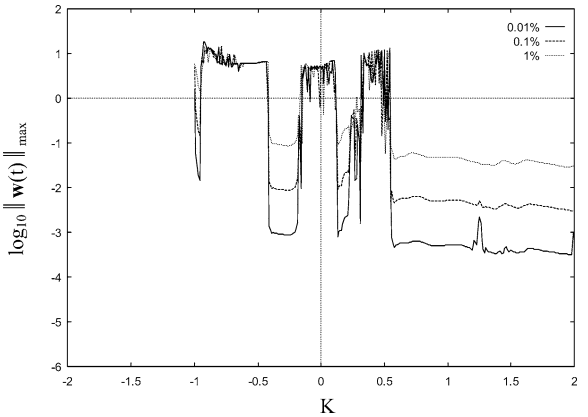

Fig. 6. Synchronization error for increasing parameter mismatch in the chaotic regime.

5. Conclusion

In this Letter, we have performed the stability analysis for the synchronization of ultra-high frequency current-modulated semiconductor lasers, both in their periodic and chaotic regimes. We have developed an approach which has resumed the stability study to a Floquet problem. Hence, we have been able to explain the occurrence of instability intervals when the parameters and/or the coupling strength are varied. We have also studied the influence of the parameter mismatch upon the quality of the synchronization.

For further investigations, several important issues remain opened. For instance, other coupling schemes can be considered. In view of applications in com-

munication engineering, a particular emphasis should also be made on the study of the delayed differential equations which enable to modelize the synchronization of (very) distant CMSLs. At last, the signal distortion due to noise and frequency filtering in telecommunication links induce a degradation of synchronization whose study should gather a specific interest.

References

[1] L.M. Pecora, T.L. Carroll, Phys. Rev. Lett. 64 (1990) 821.
[2] N.F. Rulkov, M.M. Sushchik, L.S. Tsimring, H.D.I. Abarbanel, Phys. Rev. E 51 (1995) 980.
[3] R. Fermat, J. Alvarez-Ramírez, Phys. Lett. A 236 (1997) 307.
[4] N.J. Corron, D.W. Hahs, IEEE Trans. Circuits Systems I 44 (1997) 373.
[5] B. Mensour, A. Longtin, Phys. Lett. A 244 (1998) 59.
[6] P. Woafo, Phys. Lett. A 267 (2000) 31.
[7] A. Murakami, J. Ohtsubo, Phys. Rev. E 63 (2001) 066203.
[8] A. Ritter, H. Haug, J. Opt. Soc. Am. B 10 (1993) 130.
[9] H.G. Winful, Y.C. Chen, J.M. Liu, Appl. Phys. Lett. 48 (1986) 616.
[10] M. Tang, S. Wang, Appl. Phys. Lett. 48 (1986) 900.
[11] G.P. Agrawal, Appl. Phys. Lett. 49 (1986) 1013.
[12] Y. Hori, H. Serivasa, H. Sato, J. Opt. Soc. Am. B 5 (1988) 1128.
[13] P. Ashwin, J. Buescu, I. Stewart, Phys. Lett. A 193 (1994) 126.
[14] J.F. Heagy, T.L. Carroll, L.M. Pecora, Phys. Rev. E 52 (1995) R1253.
[15] N.J. Corron, Phys. Rev. E 63 (2001) 055203.
[16] Y. Chembo Kouomou, P. Woafo, Phys. Lett. A 298 (2002) 18.
[17] P. Woafo, R.A. Kraenkel, Phys. Rev. E 65 (2002) 036225.
[18] D.J. Gauthier, J.C. Bienfang, Phys. Rev. Lett. 77 (1996) 1751.
[19] R. Brown, N.F. Rulkov, Phys. Rev. Lett. 78 (1997) 4189.
[20] C.L. Pando, Phys. Rev. E 57 (1998) 2725.
[21] G.A. Johnson, D.J. Mar, T.L. Carroll, L.M. Pecora, Phys. Rev. Lett. 80 (1998) 3956.
[22] T. Kuruvilla, V.M. Nandakumaran, Phys. Lett. A 254 (1999) 59;
V. Bindu, V.M. Nandakumaran, Phys. Lett. A 277 (2000) 345.
[23] K. Pyragas, Phys. Lett. A 181 (1993) 203.
[24] Y. Chembo Kouomou, P. Woafo, Phys. Rev. E 66 (2002) 036205.
[25] A.H. Nayfeh, D.T. Mook, Nonlinear Oscillations, Wiley, New York, 1979, Chapter 5.
[26] C. Hayashi, Nonlinear Oscillations in Physical Systems, McGraw-Hill, New York, 1964, Chapter 3.